The A Priori Design and Selection of Ionic Liquids as Solvents for Active Pharmaceutical Ingredients

Kunov-Kruse, Andreas Jonas; Weber, Cameron C.; Rogers, Robin D.; Myerson, Allan S.

Published in:
Chemistry: A European Journal

Link to article, DOI:
10.1002/chem.201605704

Publication date:
2017

Document Version
Peer reviewed version

CHEMISTRY
A European Journal

A Journal of
ChemPubSoc Europe

Accepted Article

Title: The a priori design and selection of ionic liquids as solvents for active pharmaceutical ingredients

Authors: Andreas Jonas Kunov-Kruse, Cameron Weber, Robin Rogers, and Allan Myerson

To be cited as: *Chem. Eur. J.* 10.1002/chem.201605704

Link to VoR: http://dx.doi.org/10.1002/chem.201605704

Supported by
ACES

WILEY-VCH

10.1002/chem.201605704

The *a priori* design and selection of ionic liquids as solvents for active pharmaceutical ingredients

Andreas J. Kunov-Kruse[a,b], Cameron C. Weber[a,c], Robin D. Rogers[d], Allan S. Myerson*[a]

a) Novartis-Massachusetts Institute of Technology Center for Continuous Manufacturing and Department of Chemical Engineering, Massachusetts Institute of Technology, 77 Massachusetts Avenue, Cambridge, Massachusetts 02139, United States

b) Technical University of Denmark, building 207, DK-2800 Kgs. Lyngby , Denmark

c) School of Science, Auckland University of Technology, Auckland 1010, New Zealand.

d) Department of Chemistry, McGill University, 801 Sherbrooke St. W., Montreal, QC H3A 0B8, Canada.

Abstract:

In this paper we derive a straightforward computational approach to predict the optimal ionic liquid (IL) solvent for a given compound, based on COSMO-RS calculations. These calculations were performed on 18 different active pharmaceutical ingredients (APIs) using a matrix of 240 hypothetical ILs. These results indicated that the 18 APIs could be classified into 3 distinct categories based on their relative hydrogen bond donating or accepting ability, with similar optimal IL solvent predictions within each class. Informed by these results, a family of strongly hydrogen bond donating ILs based on the *N*-alkylguanidinium cation were prepared and characterized. The solubility of the APIs in each of these classes was found to be qualitatively consistent with the predictions of the COSMO-RS model. The suitability of these novel guanidinium salts as crystallization solvents was demonstrated by the use of *N*-butylguanidinium bis(trifluoromethanesulfonyl)imide for the purification of crude fenofibrate using dimethylsulfoxide as an antisolvent, which resulted in good yields and excellent purities. Finally, a simple descriptor based model is proposed to suggest the best IL solvent for arbitrary APIs.

Introduction:

Ionic liquids (ILs) have attracted significant interest as solvents. ILs are commonly defined as salts that melt below 100 ^{o}C although many are liquid at room temperature. ILs have negligible vapor pressure and low flammability; properties that make them convenient to handle over a wide range of temperatures and process conditions.[1,2]

ILs are often referred to as “designer solvents” which arises from the flexibility of cation and anion selection which can be used in numerous ways to tailor very specific physical and chemical properties. As pointed out by Crowhurst *et al.* [3] it is still not very clear which properties can be designed into new IL systems. Furthermore the term “designer solvents” is sometimes overused and often mentioned when the ILs studied are chosen from a small number of popular commercial ILs. Part of this is due to the lack of a reliable tool to aid the search and selection of new ILs. In this paper, we will demonstrate how a straightforward combination of computational methods results in a pragmatic model which can be

applied to assess the solvation properties of hypothetical new ILs. Furthermore, the present work demonstrates how this model played a key role in the development of new ILs.

Despite the unique and tunable solvent properties of ILs, the research focused on exploiting these properties for downstream processing like purification and extraction is more limited than for applications as solvents for conducting chemical reactions, even though this is an essential part of all chemical production. A large part of the literature reporting IL separations has, until recently, mostly focused on a relatively narrow palate of techniques such as liquid-liquid extraction or membrane filtration.[4–8] Reichert *et al.*[9] discussed that the use of ILs as crystallization media is an area which has great potential, but has received very little attention. Some work has been conducted with an emphasis on the crystallization of complex molecules such as proteins[10,11] or metal-organic frameworks.[12]

Due to safety regulations, downstream processing requirements for the production of pharmaceuticals are especially stringent. Thus the separation technique must comply with very high standards for purity and polymorph control. Crystallization is often the preferred choice of purification technique in production of most Active Pharmaceutical Ingredients (APIs).[13] Despite the enormous importance of crystallization in the chemical and pharmaceutical industry, surprisingly few studies regarding API crystallization in the IL literature are concerned with this matter.

The use of ILs for the purification of APIs has not been widely investigated, with only a handful of literature reports.[14–19] Smith *et al*. investigated the solubility of ibuprofen and paracetamol in two very similar ILs, with the only difference a subtle variation of the alkyl chain length of the imidazolium cation used. Both ILs featured the same hydrophobic and weakly interacting anion $[PF_6]^-$. The scope of the study was to investigate the potential to use ILs in future crystallization processes of the two pharmaceuticals, by investigating the solubility,[14] while the group in a later paper demonstrated the crystallization of acetaminophen from the IL.[17] While these ILs are readily commercially available and comprise favorable properties like low viscosity, they may not a very good choice of ILs for the crystallization of this type of pharmaceutical, as the solubilities of most drugs are inherently low. This would require the use of large volumes of IL to be able to achieve industrially relevant quantities of crystallized API. In addition, the reactivity of the $[PF_6]^-$ anion has been reported and would be detrimental to their recyclability and long term use.[20] An *et al.* demonstrated crystallizations with excellent polymorphic control of the API adefovir dipivoxil in similar imidazolium based ILs, however again with a low API/IL ratio due to the relatively low API solubility in the used ILs.[18,19] At least at the moment ILs are still more costly than most conventionally used solvents. Thus a crystallization process based on IL solvents must offer a high purification capacity as well as efficient recyclability which is difficult if the inherent solubility of the API in the new IL solvents is low.

That the imidazolium based ILs with weakly interacting anions are quite poor solvents for APIs in general was indirectly pointed out by the latter study of Azevedo.[15] In their study, they examined the solubility of the prototype cardioactive drug LASSBio-294. They performed a qualitative analysis of hydrogen bond donor and acceptor sites of the drug and then showed that the solubility of the drug was primarily related to the hydrogen bond accepting capacity of the IL anion with alkylphosphate and acetate based ILs giving the greatest solubility. Furthermore, they demonstrated that the addition of even small amounts of water dramatically decreased the solubility, indicating these ILs may behave as useful solvents for conducting antisolvent crystallizations, although no actual crystallization was performed. These properties are analogous to the behavior of ILs studied for cellulose dissolution.[21] Our group

10.1002/chem.201605704

recently showed how IL mixtures based on 1-ethyl-3-methylimidazolium ($[EMIM]^+$) acetate ($[OAc]^-$) and bis(trifluoromethanesulfonyl)imide ($[NTf_2]^-$) ILs could be applied for the purification of crude acetaminophen by antisolvent crystallization using a sufficiently strong hydrogen bond donating antisolvent, such as 1,1,1,3,3,3-hexafluoroisopropanol.[16] The molar solubility of acetaminophen in the $[EMIM][OAc]_x[Ntf_2]_{1-x}$ mixture was found to scale linearly with the concentration of $[OAc]^-$ anions due to the formation of a postulated 2:1 hydrogen bond complex. Theoretical aspects of the acetaminophen and IL interactions were investigated by Paluch *et al.* Their results suggested that the imidazolium cation also contributed positively to the solvating effect in acetate based ILs.[22] Our group also showed that yet another possible strategy is to choose IL-API combinations with low solubility at room temperature by adopting a cooling crystallization approach.[23]

Based on the studies discussed above, ILs with good hydrogen bond accepting anions are quite often good solvents for the APIs tested, providing a high capacity to dissolve the crude API prior to recrystallization.[15,16] However, as we will demonstrate in our study, this reasoning cannot be applied to all APIs, and the IL comprising the best hydrogen bond accepting anion does not always result in high API solubility. Furthermore, it can be problematic to recrystallize an acidic API if the anion of the IL has significant Brønsted basicity.

The COnductor-Like screening MethOd for Real Solvents (COSMO-RS)[24] has successfully been demonstrated as a useful screening tool in several studies of solubilities in both neutral solvents and in ILs.[25–27] COSMO-RS requires a one-time quantum mechanical calculation to generate input files containing the polarization surface charge, the so called σ-charge, of all solutes and solvents. Once this file is generated, it can be stored in a database for later use. The software then performs an analysis of the surface interactions between solutes and solvents using statistical thermodynamics to estimate activity coefficients of the solute in the solvent at infinite dilution. A detailed description of the individual energy terms method can be found elsewhere.[24,26–29] Generally, solubilities calculated by COSMO-RS are correct only to within an order of magnitude and are most effective for determining general trends rather than absolute values. However, it should be noted that the absolute accuracy of the COSMO-RS method can be increased by using experimental values of parameters such as the enthalpy of fusion or empirical solubility points. These latter options were not used in this study owing to the lack of data available for many of the compounds examined.

Unlike many other computational chemistry methods, COSMO-RS is computationally cheap and relatively user friendly, which makes it a more attractive tool for experimental chemists and engineers. As the method is so computationally cheap, it offers a significant advantage over the more high level approaches as it can used to map a larger landscape where hundreds or even thousands of solubility scenarios can be considered simultaneously. COSMO-RS is especially convenient when working with ILs where anions and cations are treated as individual surfaces and thus a relatively modest number of representative cations and anions can be systematically combined to span a large number of potential ILs. This makes COSMO-RS interesting to use as a prescreening tool to decide on the most useful solvents to choose before starting in the laboratory, where the testing of each scenario is costly both in terms of time and resources.

This “matrix” or “map” approach has previously been demonstrated in a few studies for the solubility of biomolecules, such as cellulose[27] and selected flavonoids[26] as well as for the solubility of gases[30–32] in ILs. All of these studies used an extensive number of cation and anion combinations. The main conclusion

10.1002/chem.201605704

that can be drawn from several of these studies was that solubility could be correlated to the hydrogen bond accepting capabilities of the anion, while the cations in all these specific cases played a minor role. In this study, we have selected 15 anions and 14 cations that intentionally span a wide range of hydrogen bond donor and acceptor strengths, thus estimating the solubility of each API in 240 different ion pairs. Furthermore, we expanded our prescreening to a large and diverse group of 18 different APIs. It is important to emphasize that the purpose of the theoretical study is not to predict accurate solubilities of each API, but to establish an overview of more global solubility trends among many potential solvents and many diverse APIs. The main trends predicted with the COSMO-RS calculations were then evaluated experimentally and their use in designing a novel antisolvent crystallization process were demonstrated.

Results:

Figure 2 shows three representative examples of the solubility profiles generated by the COSMO-RS calculations. The structures of the ions used and the 18 solubility maps generated can be found in the supporting material. The map profiles for each API were subtly different, however by examining such a large number of different compounds some general patterns were noted. These patterns meant that most of the APIs could be categorized into two main types, denoted; hydrogen bond donating (HBD) and hydrogen bond accepting (HBA) APIs, the classification of which will be discussed below. Some APIs possessed significant properties from both groups and these have been denoted *hybrids.* The categorization of the 18 APIs investigated is shown in Figure 1

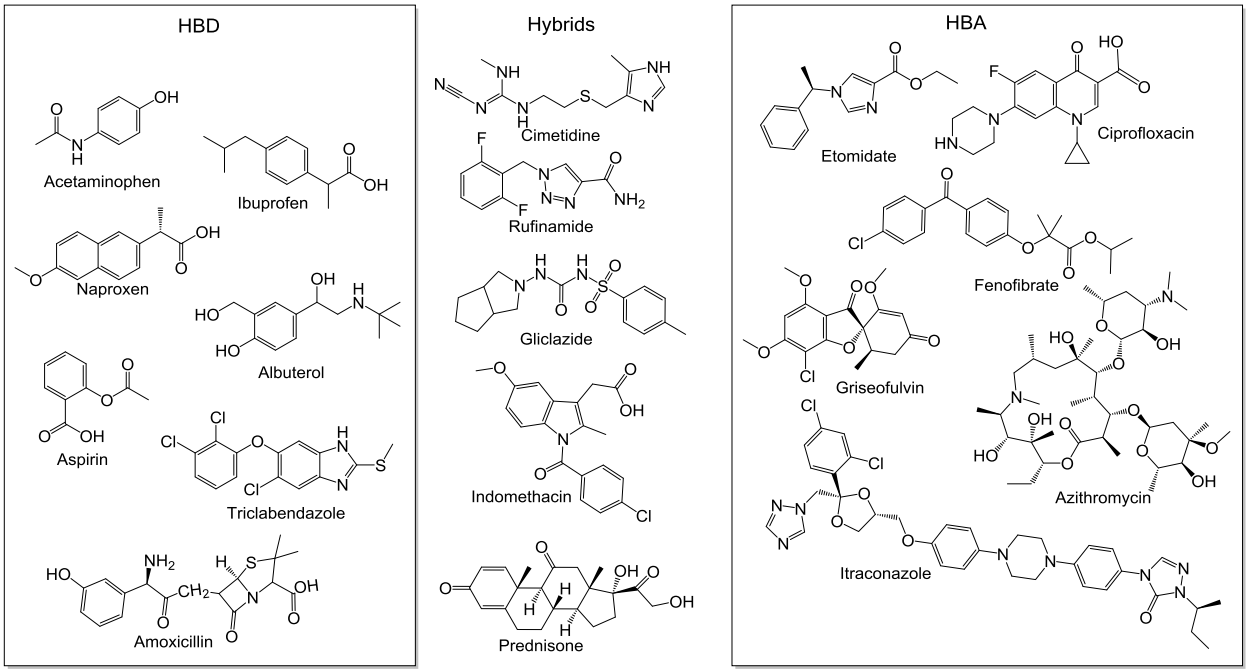

Figure 1 - An overview of all the different APIs used in the study and their classification as outlined in the text.

10.1002/chem.201605704

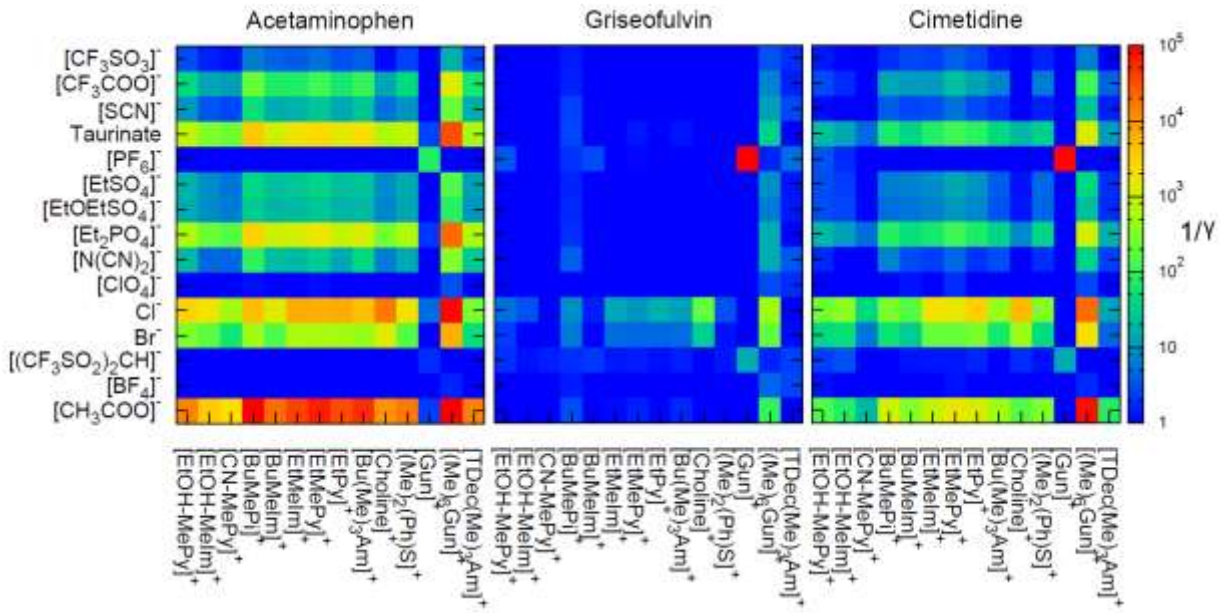

Figure 2- Three solubility maps showing estimated solubilities, as given by their reciprocal activity coefficient at infinite dilution, in 240 different ion combinations calculated by COSMO-RS. Structures of the ions and their abbreviations can be found in the supporting information. Red squares corresponds to predicted high solubilities, whereas blue correspond to very low predicted solubilities. The tree maps shows representative profiles for APIs belonging to either HBD (acetaminophen), HBA (Griseofulvin) or hybrid (Cimetidine). The solubility maps for the remaining 15 APIs investigated can be found in the supporting information.

Compounds that we have denoted HBD API's generally comprise both hydrogen bond donating and accepting sites, but their solubility is governed primarily by their hydrogen bond donating characteristics. The solubility of this group of APIs is dominated by the hydrogen bond accepting properties of the anion. Hence the best choice of solvent in terms of API solubility would be a good hydrogen bond accepting anion such as $[OAc]^-$. Similar trends were predicted and shown by Azevedo *et al.* for a single API that would be classified as HBD under this scheme.[15] APIs that have been classified as HBD include albuterol, amoxicillin, aspirin, ibuprofen, naproxen and triclabendazole.

In contrast to the existing literature which suggests ILs with strong hydrogen bond accepting anions are often the solvents with highest capacity for many APIs, a rather large group of APIs were found where the calculations suggested that such ILs would not be good solvents. We have denoted these HBA APIs. The HBA APIs include etomidate, ciprofloxacin, fenofibrate, griseofulvin, itraconazole and azithromycin. A main feature of the COSMO-RS results was that they showed the HBA APIs comprised very few or no accessible sites capable of hydrogen bond donation. These APIs represent a significant proportion of those studied, including several for which poor solubility is a common challenge both in their production as well as final application.

In some cases, HBA APIs simply lack hydrogen bond donor groups, for example griseofulvin, fenofibrate or itraconazole. In other cases, such as azithromycin, the hydrogen bond donor groups of the molecule were engaged in strong intramolecular hydrogen bonds with acceptor groups on the same molecule resulting in the overall cancelation of the net hydrogen bond donor capabilities.

For HBA APIs, the best solvent type in the matrix was the quite unusual combination of a strong hydrogen bond donating cation and a very weakly interacting anion. This type of IL is not commonly represented among commercial ionic liquids. In our hypothetical prescreening matrix, this combination

10.1002/chem.201605704

was represented by an unsubstituted guanidinium cation combined with the $[PF_6]^-$ anion. This "red point" quite early in the study caught our attention as quite unusual because the cation plays the major role in the solubility, whereas the identity of the cation is normally considered less important than that of the anion regarding solute solubility. Where cation effects are implicated, it is often argued in terms of π-π or ion-π effects in the case of aromatic solute-solvent reactions, or through indirect effects such as the influence of the cation on cation–anion association and the ability of the anion to solvate the solute.[33] Interestingly, even ion-π effects are often only indirectly linked to the cation as these have been linked with weaker cation-anion interactions and often result more from anion-π rather than cation-π type solubilization.[33,34] Part of the reason for the limited role of the cation in most systems studied are the relatively weak hydrogen bond donating properties of the typical cations used in ILs.[35–37]

More closely examining the σ-charge of the combination of a unsubstituted guanidinium cation and the $[PF_6]^-$ anion, calculated during the COSMO quantum mechanical calculations, suggests a more strongly hydrogen bond donating cation than is typically observed. The surfaces colored according to the σ-charge, denoted the σ-surface, provide an intuitive tool to understand the hydrogen bonding of both solutes and solvents. Additionally, the amount of surface area as a function of a specific surface charge density can be illustrated by what are known as σ-plots. Selected σ-surfaces and their σ-plots from this study are compared in Figure 3. From the right figure it is noticeable that the guanidinium ion is an excellent hydrogen bond donor, much better than the 1-alkyl-3-methylimidazolium ILs that are normally counted among the best hydrogen bond donating ILs.[35,37] The σ-plot also shows that the $[PF_6]^-$ anion is an exceptionally poor acceptor, making the hypothetical [Gun][PF_6] a strong hydrogen bond donor. Hence [Gun][PF_6] makes an excellent choice as a high capacity solvent for dissolving APIs that can only hydrogen bond via their hydrogen bond accepting groups, such as griseofulvin shown on the left hand side of Figure 3 which lacks hydrogen bond donating groups.

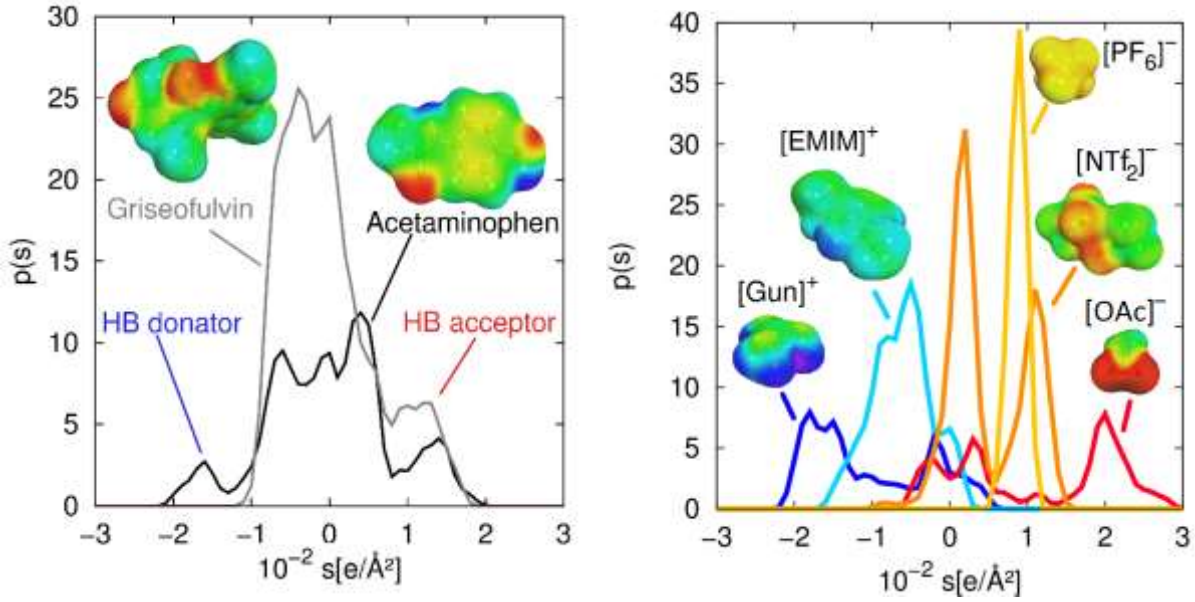

Figure 3: σ-plots and σ-surfaces surfaces obtained from the COSMO-RS calculations. Areas with a large overall positive charge density are illustrated in blue, negative charge density in red and low positive and negative charge densities in green and yellow respectively. Low electron density regions (i.e. Hydrogen bond donating sites) are depicted in blue, while high electron density regions (i.e. hydrogen bond accepting sites) in red. Left: σ-plots for two representative examples of HBD and HBA APIs. Right: σ-

plots associated with selected ions used in the calculation as well as the $[NTf_2]^-$ ion that will be described later in the experimental section.

Finally, we have placed the remaining compounds into a group we calls hybrids. They all seem to have weak to moderate hydrogen bonding capabilities through both acceptor and donor groups. Thus the COSMO-RS calculations suggests that they should have reasonable solubility in the two different archetypical ILs presented above.

From the purely quantum mechanical input COSMO-RS calculates several descriptors for each compound, called σ-moments in COSMO-RS terminology. The single value descriptors HB_don3 and HB_acc3 are of particular interest in in this study as they describe the aggregate hydrogen bond donating and accepting capacity of each compound respectively. These descriptors relate well to experimentally derived descriptors.[38–40] Examples in the literature have shown that the descriptor *HB_acc3* in particular is a good indicator for the success of IL solvents in the dissolution of cellulose and flavonoids.[26,27]

Inspired by this approach we analyzed the descriptor values of archetypal HBD and HBA APIs, to see if these descriptors could be used to assign them to either of the two groups. As the molecules differ greatly in size we normalized the descriptors with respect to the cavity volume of the compound, see Table 1. We could observe that no clear trend could be found based on either of the two descriptors alone, and the group assignment seemed to rely more on the ratio between two descriptors. Thus we finally found that the logarithm to the ratio between HB_don3 and HB_acc3 correlated well with our classification system. This ratio is straightforward to calculate for APIs and, given the similarity of COSMO-RS results for each classification of API, makes the COSMO-RS prescreening method even more practical as it does not require setting up a large matrix of ions. Based on our classification system we found that APIs with log(HB_acc3/HB_don3) < 0 seem to belong to the HBD category, while the compounds with log(HB_acc3/HB_don3) > 1 belong to HBA, with intermediate values belonging to the Hybrid category.

*Table 1 - Overview of important key values for the different APIs used in the study. [a)]HB_acc3 and HB_don3 descriptor values taken from COSMOtherm calculations. As the descriptors are size dependent, these are normalized with respect to the volume of the cavity and are given in 10^{-2} Å^{-3}. Where relevant, the pK_a values are also given. Unless otherwise stated all melting points and pK_a values are experimental and are taken from [41,42] and references herein. [b)]*Non-Steroidal Anti-Inflammatory Drug

API	log(HB_acc3/HB_don3)	Classification	PK_a	Relative HB_acc3 [a]	Relative Hb_don3 [a]	MP (°C)	API use
Acetaminophen	-0.11	HBD	9.9	2.39	3.10	170	Pain reliever and fever reducer
Albuterol	-0.10	HBD	9.3	1.63	2.07	148	Asthma
Amoxicillin	-0.10	HBD	2.4	1.23	1.56	194	Antibiotic
Aspirin	-0.37	HBD	3.5	0.83	1.97	135	NSAID [b)]
Ibuprofen	-0.45	HBD	5.2	0.49	1.37	76	NSAID [b)]
Triclabendazole	-0.46	HBD	-	0.36	1.06	176	Anthelmintics
Naproxen	-0.37	HBD	4.2	0.58	1.38	153	NSAID [b)]

10.1002/chem.201605704

Indomethacin	-0.12	HBD	4.5	0.75	0.99	151	NSAID [b)]
Rufinamide	0.35	Hybrid	-	1.71	0.77	239	Anticonvulsant
Cimetidine	0.35	Hybrid	6.8	2.44	1.09	142	Histamine H2-receptor antagonist
Gliclazide	0.58	Hybrid	5.8[43]	0.79	0.21	180	Hypoglycemic
Prednisone	0.54	Hybrid	-	2.06	0.60	233	Corticosteroid
Azithromycin	1.37	HBA	-	1.28	0.06	114	Antibiotic
Ciprofloxacin	1.82	HBA	6.09	1.76	0.03	256	Antibiotic
Etomidate	2.27	HBA	-	2.08	0.01	142	Anesthetic agent
Fenofibrate	2.02	HBA	-	0.72	0.01	80	Cholesterol reducing
Griseofulvin	1.36	HBA	-	1.54	0.07	220	Antifungal
Itraconazole	1.65	HBA	-	1.27	0.03	166	Antifungal

To experimentally verify that the COSMO-RS predictions were accurate, it was necessary to investigate the synthesis of representative guanidinium based ILs. Unfortunately, not all ion combinations in the matrix are ILs – in fact a lot of the combinations are salts melting at high temperatures. On this basis several of the good candidates could be eliminated. Initially the promising [Gun][PF_6] was synthesized and found to have a high melting point. Initially attempts were made to prepare mixtures with [EMIM][NTf_2] but they were unsuccessful as the guanidinium salt decomposed on dissolution. The anion on the guanidinium salt was then replaced by $[NTf_2]^-$ which is also weakly interacting like $[PF_6]^-$ (see Figure 3) but is more stable and tends to form salts with lower melting points. The resultant salt, [Gun][NTf_2], was synthesized and melted around 90-95 ^oC, which is not convenient for a recrystallization medium in an industrial downstream process. In order to further reduce the melting point, an alkyl side chain was introduced on the cation and the ethyl-, propyl- and butylguanidinium analogs were prepared (denoted $[EtGun]^+$,$[PrGun]^+$ and $[BuGun]^+$ respectively, Figure 4). While $[EtGun]^+$ was available commercially, $[PrGun]^+$ and $[BuGun]^+$ cations could be synthesized from the reaction of the corresponding the alkylamine with O-methyl-isourea sulfate in water.[44]

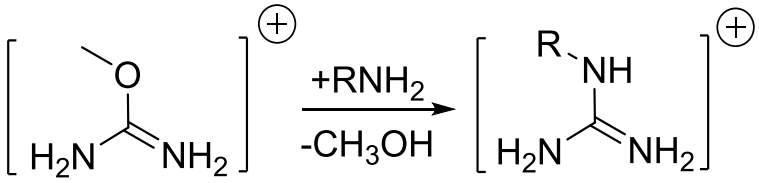

Scheme 1. Synthesis of alkylguanidinium salts.

This simple route avoids the many complex synthesis steps and the consequently high E-factor often associated with guanidinium derivative synthesis. The corresponding $[NTf_2]^-$ salts could then be prepared by the addition of aqueous Li[NTf_2] to an aqueous solution of the alkylguanidinium sulfate salt, with the alkylguanidinium [NTf_2] separating from the aqueous phase. Washing the IL phase, or the IL dissolved in dichloromethane, with water enabled the removal of residual sulfate anions and the isolation of the pure alkylguanidinium [NTf_2] salt.

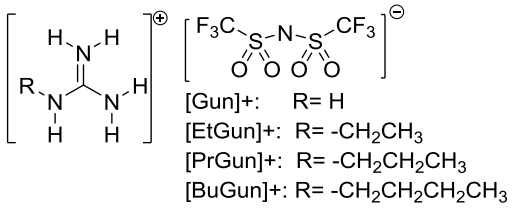

Figure 4 – The structure of the guanidinium $[NTf_2]^-$ based ILs and their abbreviations.

This synthetic approach turned out to be successful with good to excellent yields resulting for the $[PrGun][NTf_2]$ and $[BuGun][NTf_2]$. The yield was much lower for $[Gun][NTf_2]$ and $[EtGun][NTf_2]$ due to their higher aqueous solubility. An interesting aspect is that while this synthesis procedure is a convenient, however slightly expensive synthesis on a lab scale, a much cheaper and equally simple synthesis using S-methyl-isourea could be used to produce the IL on an industrial scale.[44] The melting points of the resultant ILs decreased with increasing alkyl chain, with $[BuGun][NTf_2]$ being liquid at room temperature (Table 2).

Table 2 - The melting points of the synthesized $[RGun][NTf_2]$ ILs.

Ionic liquid	**Melting point**
$[Gun][NTf_2]$	>90°C
$[EtGun][NTf_2]$	81°C
$[PrGun][NTf_2]$	39°C
$[BuGun][NTf_2]$	18°C

The use of guanidinium derived ILs is not entirely new, and different highly *N*-substituted ILs are described in several studies and references therein.[36,45–49] . Highly substituted guanidine/alcohol mixtures has also been used in switchable solvent systems, which reversible transforms into ionic liquids upon addition of CO_2 [50].

However the highly substituted guanidinium ions have very different properties from those with a low degree of substitution presented in our study. Depending on the anion used as well as the method used for their characterization, studies have shown hexaalkylguanidinium based ILs either behave similarly to analogous imidazolium based ILs,[36,46] or in other cases as significantly less polar.[45] In either case these cations behave very differently to the monosubstituted guanidinium ILs. This seems to be a consequence of the changing electrostatic properties as the positive charge is dispersed over a larger region and the cation becomes a much poorer hydrogen bond donor due to the lack of availability of hydrogens directly bound to the nitrogen.

Another well described family of guanidinium cations are those based on the tetramethyl guanidinium cation, which relates to the fact that tetramethylguanidine is cheap and commercially available as it is a widely used industrial base. Tetramethyl substituted guanidinium derived ILs and salts have been used as reaction media in organic synthesis,[51] SO_2 capture[52,53] and as electrolytes.[47]

10.1002/chem.201605704

The new ILs we present in this work are based on singly substituted guanidinium cations, which leads them to possess different properties to the highly substituted ILs described above. To the best of our knowledge, such monoalkyl guanidinium ILs have not been described in the IL literature although there are a number of studies concerned with similar salts bearing different anions in the biochemistry literature.[54–58] Monoalkylguanidines are strong Brønsted bases like guanidine,[59] giving the corresponding guanidinium ions negligible Brønsted acidity and thus forming stable cations. As these are a new class of IL cation, it was of interest to compare the solvent properties of these ILs with other commonly used cations. Solvent polarity, particularly within ILs, is often described using the multiple parameter approach initially described by Kamlet and Taft.[3,35,37,60]The Kamlet-Taft parameters α, β and π* refer to the hydrogen bond acidity, hydrogen bond basicity and dipolarity and polarizability of the solvent respectively. These are determined experimentally through the use of solvatochromic dyes. Several studies have shown that these parameters correlate reasonably well with the HB_don3 and HB_acc3 descriptors obtained computationally using COSMO-RS.[38–40,61] Furthermore, several other studies have found that it is possible calculate other theoretical descriptors that correlate well with the Kamlet Taft parameters, e.g. probes in simple DFT calculations [62] or by extracting interaction energy terms from COSMO-RS calculations.[25,63]

The HB_don3 values in Table 3 strongly suggests that $[Gun]^+$ and $[BuGun]^+$ cations are by far the best hydrogen bond donors examined, in stark contrast with the fully substituted guanidinium ILs examined. As this lies outside of the previous correlations conducted for α parameters, we have not attempted to convert this into a quantitative α value although note that it would be much higher than the conventionally used imidazolium ILs. This suggests that these monoalkylguanidinium ILs possess a similarly strong hydrogen bond donating ability as the unsubstituted guanidinium cation which they were synthesized to model. The same conclusion can clearly be made from the σ-profiles of selected cations shown in Figure 4

Table 3 - HB_don3 descriptor of selected cations calculated using COSMOtherm. : 1-butyl-3-methylimidazolium [BMIM], 1-butyl-4-methylpyridinium [BMPy], N-Ethyl-N-methylpiperidinium [EMPip], N-butyl-methylpiperidinium [BMPip], hexamethylguanidinium [Me_6Gun], 1,1-dibutyl-2,2,3,3-tetramethylguanidinium [Bu2Me4Gun]

IL cations	HB_don3
$[Gun]^+$	22
$[BuGun]^+$	16
$[EMIM]^+$	2.0
$[BMIM]^+$	1.9
$[BMPy]^+$	0.91
$[EMPip]^+$	0.15
$[BMPip]^+$	0.15
$[Me_6Gun]^+$	0.0
$[Bu_2Me_4Gun]^+$	0.0

10.1002/chem.201605704

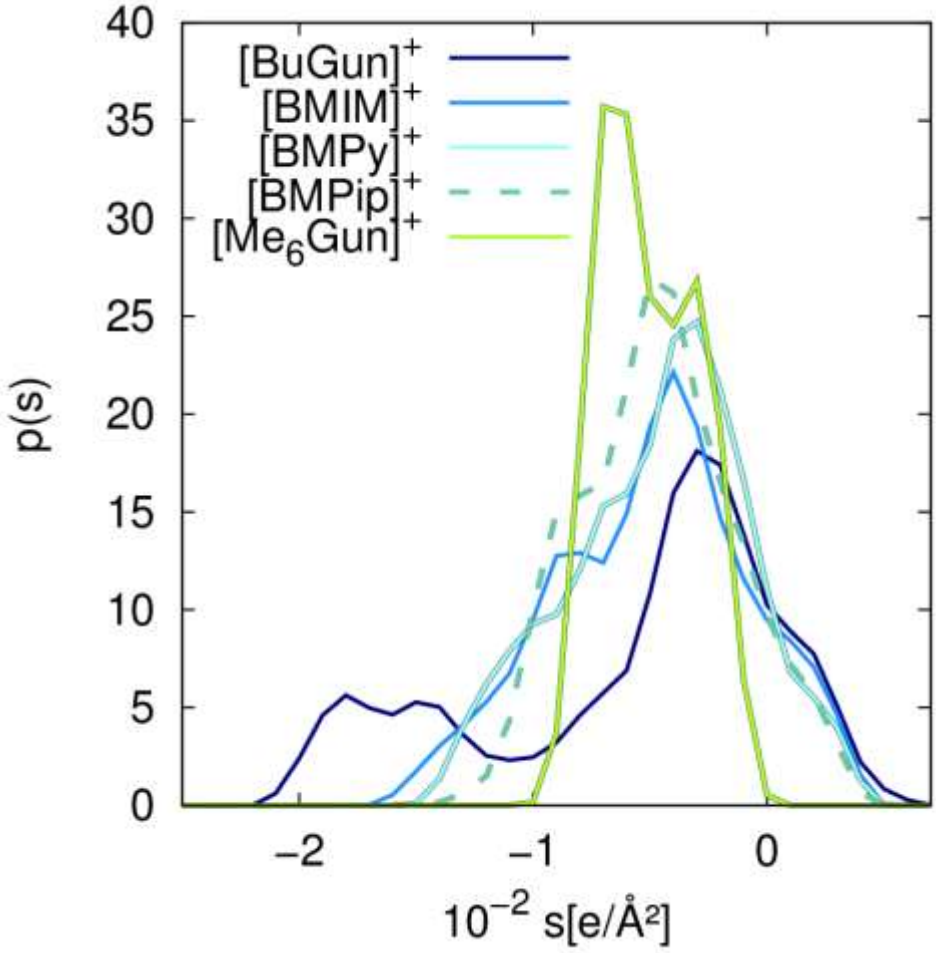

Figure 4 – Comparison of σ-profiles of selected cations.

Having prepared [BuGun][NTf_2] as a good representative for the hypothetical [Gun][PF_6] IL used in the COSMO-RS calculations, the predictions of the COSMO-RS screening study were investigated by measuring the experimental solubility of the APIs (Figure 5). The sequence of the APIs in the plot follows the value of the descriptor log(HB_acc3/HB_don3) discussed previously. The most negative values for HBD compounds are on the top left and the highest positive values for HBA compounds on the bottom right.

10.1002/chem.201605704

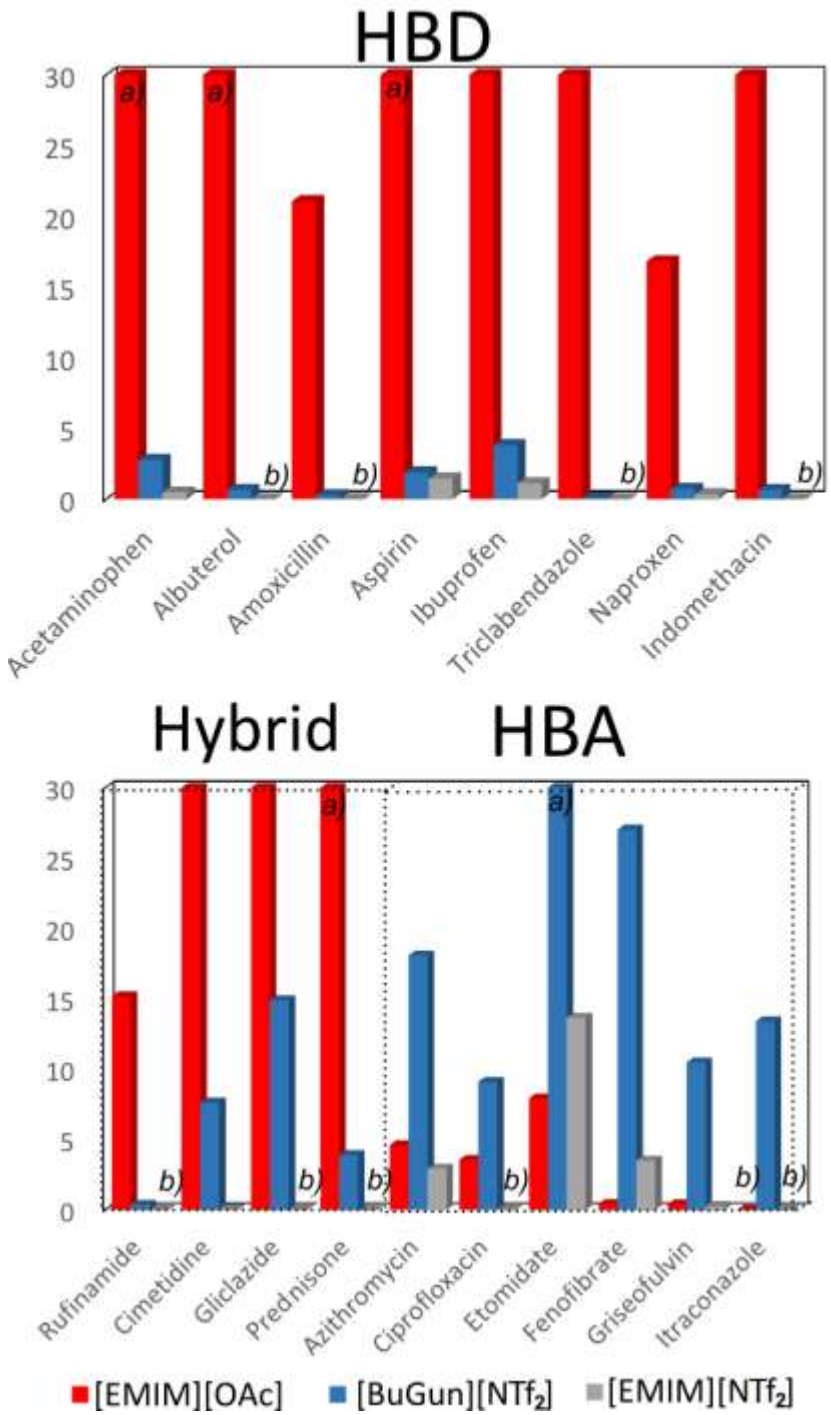

Figure 5- Experimental solubilities in wt% for [EMIM][OAc], [BuGun][NTf_2] and [EMIM][NTf_2] at 25°C measured by ^{1}H-NMR. For some of the APIs it was not possible to measure a finite solubility, as the IL became to viscous to stir at high concentrations of solute. All these were above a threshold of 30 wt.% API and are denoted by a). In some cases where the solubility was below the limit of detection, these are denoted by b).

Along with the new highly hydrogen bond donating IL [BuGun][NTf_2], the commercially available and widely used [EMIM][OAc] was chosen as the archetypal strong hydrogen bond accepting IL. To exclude

10.1002/chem.201605704

any active solubilizing effect of either the $[EMIM]^+$ or the $[NTf_2]^-$ ions in the two ILs above, $[EMIM][NTf_2]$ was chosen as a control solvent.

The importance of the hydrogen bond accepting anion among the HBD compounds was very well predicted by COSMO-RS with very high solubilities of these compounds in [EMIM][OAc] with generally low solubilities in the other ILs. Admittedly, some of the extraordinary high solubilities in the HBD group would be enhanced due to deprotonation of the APIs, which is not considered in our simplified COSMO-RS calculations. As mentioned earlier, the role of ILs with strong hydrogen bond accepting anions as good solvents for compounds with strong hydrogen bond donating sites is quite well established.

The solubilities of HBA APIs behaved as predicted by COSMO-RS. The solubilities were generally low in [EMIM][OAc] with high solubilities observed in$[BuGun][NTf_2]$. The control experiments with $[EMIM][NTf_2]$ showed that the high solubility could be predominantly related to the strong hydrogen bond donating $[BuGun]^+$ cation rather than a direct role of the $[NTf_2]^-$ anion, as would be expected.

The last group comprising APIs that were categorized as hybrids between the two groups acted as expected with fairly high solubilities found for both $[BuGun][NTf_2]$ and [EMIM][OAc] in most cases. The major exception was rufinamide which was almost insoluble in $[BuGun][NTf_2]$ but highly soluble in [EMIM][OAc]. Notably rufinamide was the most 'HBD' like of the hybrid APIs which could account for this behavior. These experimental solubilities indicate that the COSMO-RS screening provided an excellent qualitative tool for the prediction of appropriate ILs to provide high solubilities of these APIs.

In order to assess the efficacy of the novel IL $[BuGun][NTf_2]$ as a crystallization solvent for these HBA APIs, fenofibrate was chosen as a model API. A major impurity in fenofibrate is the corresponding carboxylic acid, often called fenofibric acid (Figure 6).

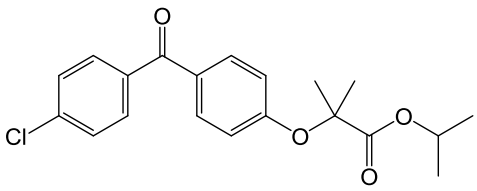

Fenofibrate

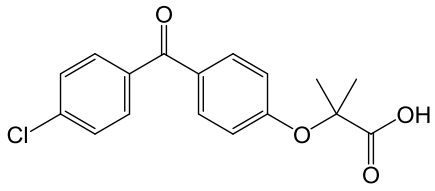

Fenofibric acid

Figure 6 - Structures of fenofibrate and fenofibric acid.

The antisolvent was selected based on the following criteria: 1) The antisolvent should form strong hydrogen bonds with the $[BuGun]^+$ cation, hence be a good acceptor, 2) the solubility of the impurity in the antisolvent should be sufficiently high to prevent its coprecipitation, and 3) the antisolvent should preferably be a benign non-toxic solvent (FDA Class III). Dimethylsulfoxide (DMSO) turned out to fulfill all of the above three criteria. Ethanol as a much weaker hydrogen bond accepting solvent was chosen for comparison.

10.1002/chem.201605704

The crystallizations were performed using a 20 % wt. solution of "crude" fenofibrate (fenofibrate mixed with 10 wt.% fenofibric acid) in freshly dried [BuGun][NTf_2]. The yield and purities were calculated from HPLC analysis (Table 4). The results show that the DMSO indeed induces a selective antisolvent effect that causes a large amount of the fenofibrate to crystallize while retaining the fenofibric acid impurity in solution. While the purity was very high in the crystallized product even at low DMSO ratios, the yield started dropping dramatically as the concentration of DMSO increased, indicating that DMSO beyond a certain point would start to act as a co-solvent instead of an antisolvent. Given the high yields at low volumes of DMSO, this implies a specific hydrogen bond complex with the $[BuGun]^+$ cation forms to competitively reduce the solvation of fenofibrate. The low yield when using ethanol as antisolvent shows that is a much weaker hydrogen bond acceptor than DMSO. It should be noted that these crystallizations were conducted isothermally and have not been optimized, meaning that even greater yields could potentially be obtained by performing cooling antisolvent crystallizations or varying the temperature of the antisolvent crystallization.

Table 4 - The yield and purity determined for the antisolvent crystallizations of fenofibrate in [BuGun][NTf2] at 25°C

IL:AS ratio	Purity	Yield
1IL :2 DMSO	99.4%	65.6%
1IL :4 DMSO	99.7%	63.7%
1IL :6 DMSO	99.8%	41.1%
1IL :6 EtOH	99.9%	12.7%

The DMSO-cation interactions were investigated using ATR-FTIR (Figure 7). Assignments of non-obvious spectroscopic modes and their shift were performed on the basis of DFT calculated IR spectra, which can be found in the supporting information. Initially the interaction between the cation and DMSO was probed by observing the N-H stretching region. Following the addition of the first two mole equivalents of DMSO a pronounced redshift of the intense ν_{NH} modes of the guanidinium cation occurs along with a new low wavenumber mode at around 3150 cm^{-1}, indicating formation of strong hydrogen bonds with the DMSO. The band assigned to N-H hydrogen bonding with the oxygen of DMSO, corresponds very closely to that predicted in the DFT calculation of the DMSO complex(see ESI figures S21-S25 and S28-S29). Beyond 2 mole equivalents the spectroscopic signature of the DMSO-$[BuGun]^+$ complex does not significantly change and beyond 3 mole equivalents the changes in the spectra can exclusively be attributed to the dilution of the $[BuGun]^+$-DMSO complex. This also explains why the yield of fenofibrate decreased at ratios of DMSO to [BuGun][NTf_2] greater than 2:1, as the DMSO is no longer engaging in hydrogen bonding with the cation complex and hence would begin to solvate the fenofibrate.

Spectra were also obtained of the fenofibrate-[BuGun][NTf_2] solutions right after antisolvent addition, before any crystallization had occurred (Figure 8, right). The strongest hydrogen bond accepting site on the fenofibrate is the carbonyl group. The carbonyl stretch in the initial fenofibrate-[BuGun][NTf_2] solution is observed at around 1717 cm^{-1} ($\nu_{C=O}$). Upon addition of DMSO to the solution a dramatic blueshift in the fenofibrate $\nu_{C=O}$ band to around 1728 cm^{-1} occurred. This is consistent with the occupation of the cation N-H sites by the stronger hydrogen bond accepting DMSO S=O oxygen, selectively breaking the H-bonds between the fenofibrate and the guanidinium N-H groups. At one mole

10.1002/chem.201605704

equivalent the exclusion of the fenofibrate carbonyl group from the guanidinium N-H was almost complete, indicating that one DMSO molecule is capable of stoichiometrically binding one $[BuGun]^+$ cation. The blueshift in the carbonyl C=O stretching band is well supported by the DFT simulated spectra (see supporting information S26-S27)

Comparing the DMSO IR results with those containing ethanol and the fenofibrate-$[BuGun][NTf_2]$ solution (Figure 8, left) no strong hydrogen bonding effects were observed; instead, the spectra indicate a competitive equilibrium between the carbonyl-cation and the ethanol-cation complexes, explaining why the antisolvent effect is so much weaker. This demonstrates that the hydrogen bonding in the *N*-alkylguanidinium based ILs can be interrupted easily by the correct choice of antisolvent and that this selection should be guided by considering the molecular interactions involved not the absolute solubility of the solute in the antisolvent. This is conceptually similar to the approach we have examined previously with the use of hydrogen bond donating antisolvents to compete with HBD type solutes.[16]

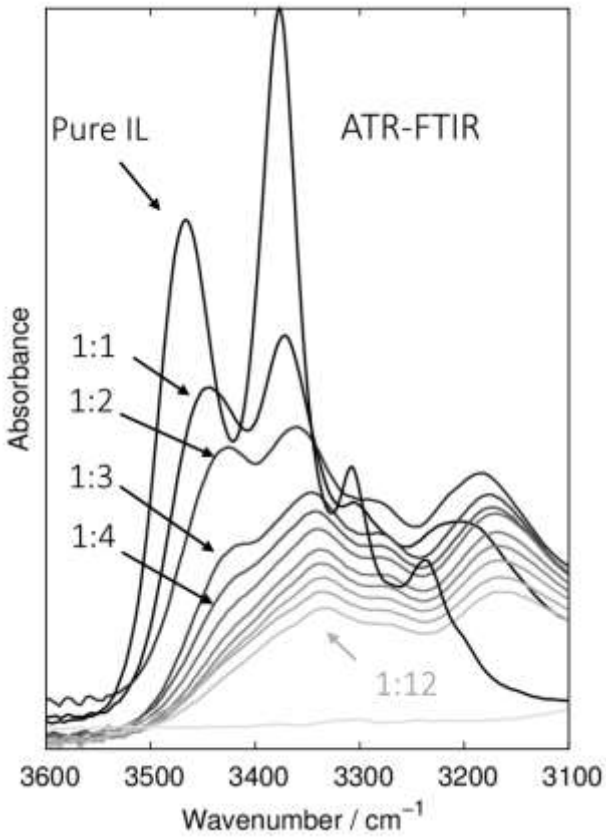

Figure 7 - ATR-FTIR spectra in the N-H and C-H stretching region of mixtures of $[BuGun][NTf_2]$ and DMSO at different molar rations from the pure IL up to a 1:12 molar dilution with DMSO. The darker tones correspond to the pure and less diluted IL samples. The lower light grey spectrum is pure DMSO.

10.1002/chem.201605704

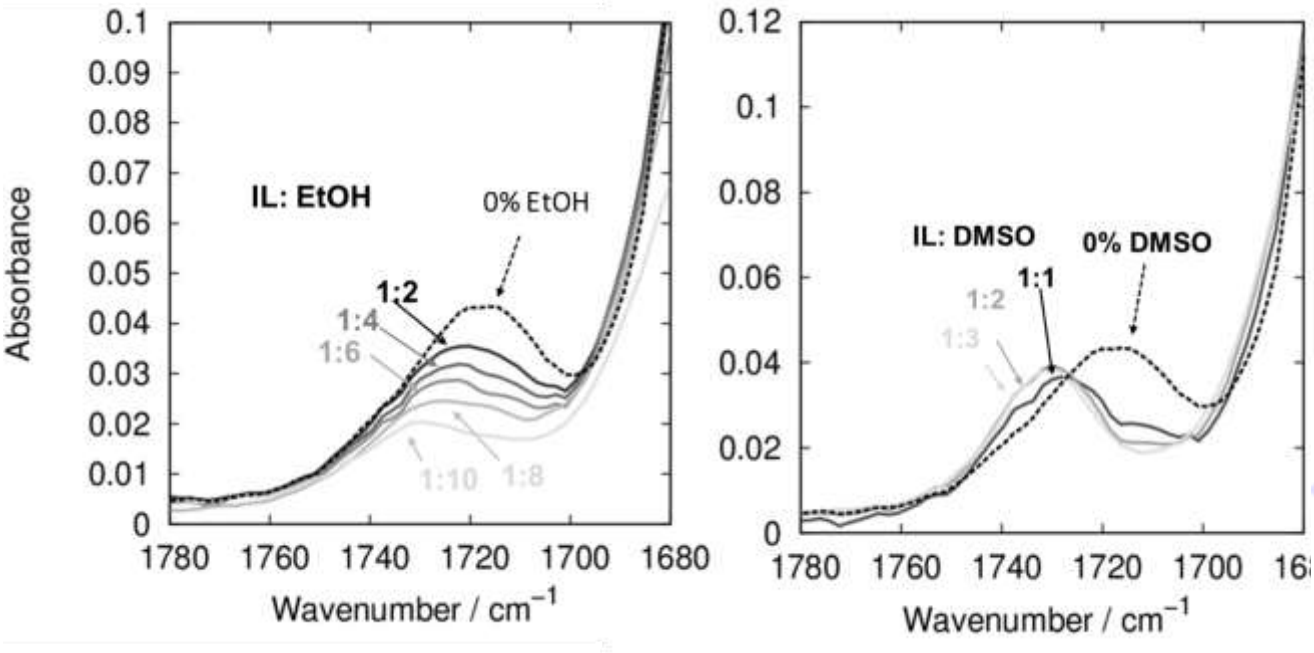

Figure 8 ATR-FTIR spectra comparing the antisolvent effect on the fenofibrate-[BuGun][NTf_2] system by using the fenofibrate carboxylic stretching as a probe. The left hand side spectra show the weak effect of adding ethanol wheras the right hand side shows the much more profound effect of adding DMSO.

As an interesting side note, [BuGun][NTf_2] was found to dissolve precisely 1 molar equivalent of water at room temperature despite being immiscible with bulk water. The hydrated IL seems to possess different physicochemical properties to the anhydrous [BuGun][NTf_2]. For example, the anhydrous IL was fully miscible with dichloromethane, whereas the hydrate was immiscible. This tunable solvophobicity is described in greater detail in the supporting information.

Conclusions:

We have demonstrated an approach to select IL solvents for the solubilisation of APIs, based on COSMO-RS computations. Based on the analysis of 18 different APIs, all compounds exhibited one of two major solubility trends or aspects of both which we categorized as HBD, HBA and hybrid. HBD APIs were characterized by sites that were significant hydrogen bond donors, and the calculations suggested that the hydrogen bond acceptor capability of the IL anion was most important to ensure high solubility. HBA APIs were characterized by partial or complete the lack of accessible hydrogen donating sites. In this case the model suggested the best IL solvents comprise a strong hydrogen bond donating cation and a weakly interacting anion. Based on these suggestions we synthesized a new family of ILs based on N-alkylguanidinium cations and the $[NTf_2]^-$ anion. The calculated solubility trends and the proposed categorization system was tested experimentally by measuring the solubilities of the 18 APIs in [BuGun][NTf_2], [EMIM][OAc] and [EMIM][NTf_2], which showed the proposed model is an effective predictor of optimal solvent selection. Further we have derived a useful and very simple descriptor log(HB_acc3/HB_don3) to classify APIs into each of the relevant categories. This descriptor can easily be calculated using COSMO-RS software, and should be applicable to all organic compounds, not just

limited to APIs, and hence could serve as a more general methodology for determining the optimal IL solvent for a given solute.

The use of [BuGun][NTf_2] as a solvent for the purification of fenofibrate by antisolvent crystallization was demonstrated. The study showed that it was possible to manipulate the hydrogen bonding in the IL by a rational choice of antisolvent, where the hydrogen bond donating sites of the cation could be selectively occupied by the addition of DMSO. The hydrogen bonding underlying the dissolution of fenofibrate as well as the antisolvent mechanism was elucidated by ATR-FTIR spectroscopy. The antisolvent crystallization experiments with DMSO resulted in fenofibrate produced in good yields and excellent purity. Given the solubility of APIs appears to fall into two distinct classes, albeit with some overlap between the two, and it appears possible to use an antisolvent with complementary hydrogen bonding capabilities to the IL to achieve good isothermal antisolvent crystallisation yields; these results define a series of straightforward rules for the selection of optimal IL solvents and antisolvents. This selection can be achieved on the basis of a simple and rapid computation (i.e. that of log(HB_acc3/HB_don3)) and should be applicable to all organic solid solutes, not necessarily just APIs. Consequently, here we have defined a straightforward and general methodology by which IL solvents and antisolvents can be selected for the purification of organic solids by crystallization.

Computational:

All COSMO-RS calculations were performed using COSMOthermX version 14 using the TZVP parameterization. All the ion and compounds *.cosmo files found in the COSMOlogic databases were used as received, while the *.cosmo files for the remaining ion and solute data were generated using the BP86 functional together with the TZVP basis set. Gaussian09 was applied for structure optimization and Gaussian03 to generate the COSMO files.

Calculation of the vibrational modes and their IR activity was also performed using the BP86 functional in combination with the TZVP basis set using a scaling factor of 1.028. The simplest model that was found to successfully describe the experimental spectra of [BuGun][NTf_2] was a cluster comprising two ion pairs. As the environment of the fenofibrate was probed using its C=O stretching band, an isopropyl 2-methoxy-2-methylpropanoate fragment was used as a model in combination with the [BuGun][NTf_2] ion-pair dimer. For complex structures the force constants were calculated at the beginning of the optimization. Screenshots of the optimized structures and theoretical IR spectra can be found in the supporting material.

Experimental:

Melting points were determined visually by adding a small sample of IL to a sealed vial and raising the temperature of a water bath in 1^{o}C steps.

Ionic liquid Synthesis:

[Gun][PF_6]:

[Gun][PF_6] was synthesized by refluxing [Gun]Cl (20.0 g, 0.21 mol) (Sigma-Aldrich) and KPF_6 (38.5 g, 0.21 mol) (Sigma-Aldrich) in acetone (150 mL) for 1 week. The suspension was filtered and [Gun][PF_6] was

obtained as a white solid by evaporation of the acetone under reduced pressure. The salt still contained some chloride impurities ($AgNO_3$ test), however due to its high melting point and low stability no further attempts were made to purify or characterize this compound.

[Gun][NTf_2]:

[Gun]Cl (20 g, 0.21 mol) and lithium bis(trifluoromethylsulfonyl)imide (60.3 g, 0.21 mol) (Io-li-tec) were each dissolved in the minimal amount of water. They were then combined resulting in a waxy white precipitate which was washed with a small amount of water. The precipitate was purified by dissolving it in acetone and standing at –20 °C to facilitate precipitation of LiCl before the solid was removed by filtration. [Gun][NTf_2] (31 g, 0.09 mol, 43 % yield) was obtained as a white solid by evaporation of the acetone. Some chloride impurity was observed by the formation of a slightly milky solution when testing with an aqueous solution of $AgNO_3$. However, the chloride content was found to be less than 0.1% w/w determined gravimetrically after the quantitative precipitation with an aqueous solution of $AgNO_3$.

[EtGun][NTf_2]:

Bis(Ethylguanidinium) sulfate (25.4 g, 0.295 mol) (Alfa Aesar) was dissolved in a small amount of water and mixed with a concentrated solution containing a half molar equivalent of lithium bis(trifluoromethylsulfonyl)imide (42.4 g, 0.148 mol). [EtGun][NTf_2] separated as colorless crystals, which melted upon gentle heating of the solution forming a second liquid phase with water. The aqueous phase was removed, and the IL phase was washed 3 times with water before being dried *in vacuo* resulting in the formation of [EtGun][NTf_2] as a white solid (9.1 g, 0.0248 mol, 8.4 %) with a melting point of 80-81^{o}C. The low yield seems to occur from heavy loss during the washing steps.

No sulfate could be detected by testing with a 0.1 M $BaCl_2$ solution.

MS (ESI +) (*m/z* (%)) 88.1 ([EtGun]$^+$, 100). (ESI −) (*m/z* (%)) 279.8 ([NTf_2]$^-$, 100). ^{1}H NMR δ (ppm) (400 MHz, acetone-d_6) 6.00-8.00 (br s, 4H, N*H*), 3.42 (q, 2H, $^3J_{HH}$ = 7.2 Hz, CH_2), 1.26 (t, 3H, $^3J_{HH}$ = 7.2 Hz, CH_3). ^{13}C{^{1}H} NMR δ (ppm) (101 MHz, acetone-d_6) 158.05 (s, N*C*), 121.10 (q, $^1J_{CF}$ = 320 Hz, *C*F_3), 37.51 (s, *C*H_2), 14.36 (s, *C*H_3). ^{19}F{^{1}H} NMR δ (ppm) −79.96 (s, CF_3).

[PrGun][NTf_2] and [BuGun][NTf_2]

In a typical synthesis, the relevant alkylamine (1.05 equivalents) and 120.0 g O-methylisourea hemisulfate salt (Alfa Aesar 99%) were refluxed in water for 1 week to ensure complete reaction. A concentrated aqueous solution of an equivalent lithium bis(trifluoromethanesulfonyl)imide (≈50 wt. %) was added in excess to the alkylguanidinium sulfate solution under rapid stirring which resulted in the formation of an IL rich bottom phase. Dichloromethane was added to increase the volume of the IL phase and the organic phase washed with water. After three to five extractions, the ILs tested sulfate free by dissolving a sample of IL in a 0.1 M $BaCl_2$ solution. The ILs were subsequently dried *in vacuo* to produce the resultant compounds as clear, colorless liquids.

[PrGun][NTf_2] (Yield 71%) (m.p. 39 °C) MS (ESI +) (*m/z* (%)) 102.1 ([PrGun]$^+$, 100). (ESI −) (*m/z* (%)) 279.8 ([NTf_2]$^-$, 100). ^{1}H NMR δ (ppm) (400 MHz, acetone-d_6) 6.20-7.80 (br s, 4H, N*H*), 3.33 (q, 2H, $^3J_{HH}$ = 7.2 Hz, NCH_2), 1.67 (sextet, 2H, $^3J_{HH}$ = 7.2 Hz, NCH_2CH_2), 0.96 (t, 3H, $^3J_{HH}$ = 7.2 Hz, CH_3). ^{13}C{^{1}H} NMR δ (ppm) (101 MHz, acetone-d_6) 158.21 (s, N*C*), 121.06 (q, $^1J_{CF}$ = 320 Hz, *C*F_3), 44.16 (s, NCH_2), 22.84 (s, NCH_2CH_2), 11.28 (s, *C*H_3). ^{19}F{^{1}H} NMR δ (ppm) −79.95 (s, CF_3).

10.1002/chem.201605704

[BuGun][NTf_2] (Yield 90 %) (m.p. 18 °C) MS (ESI +) (*m/z* (%)) 116.1 ([BuGun]$^+$, 100). (ESI −) (*m/z* (%)) 279.8 ([NTf_2]$^-$, 100). ^{1}H NMR δ (ppm) (400 MHz, acetone-d_6) 6.20-7.80 (br s, 4H, N*H*), 3.36 (q, 2H, $^3J_{HH}$ = 7.2 Hz, NCH_2), 1.63 (quintet, 2H, $^3J_{HH}$ = 7.2 Hz, NCH_2CH_2), 1.40 (sextet, $^3J_{HH}$ = 7.2 Hz, CH_2CH_3), 0.92 (t, 3H, $^3J_{HH}$ = 7.2 Hz, CH_3). ^{13}C{^{1}H} NMR δ (ppm) (101 MHz, acetone-d_6) 158.15 (s, N*C*), 121.00 (q, $^1J_{CF}$ = 320 Hz, CF_3), 42.27 (s, NCH_2), 31.49 (s, NCH_2CH_2), 20.39 (s, CH_2CH_3), 13.84 (s, CH_3). ^{19}F{^{1}H} NMR δ (ppm) −79.94 (s, CF_3).

Single X-Ray structures of the dry and 'wet' [EtGun][NTf_2] was performed by Dr. Peter Muller at the MIT single X-ray facility as described elsewhere.[64] The crystal structure including the complete structural details are shown in the supporting information and in the attached Crystallographic Information File.

Solubility:

For solubility testing 1 mL of IL was transferred to a vial with API and a small rare earth Teflon coated magnetic stirrer. All samples were then placed in an aluminum block maintained at 25.0 °C overnight with stirring. If the API completely dissolved more was gradually added until the solution was saturated. [EMIM][OAc] could dissolve very large amounts of some of the HBD APIs until it formed a viscous clear solution that could no longer be stirred. In these cases, it was not practical to obtain saturation and determine the true solubility, as has been noted in the text.

After a saturated solution was obtained, the IL was filtered slowly using a syringe filter (Tuffryn 0.4µm) and a few drops was transferred to a vial and mixed with DMSO-d_6. The ^{1}H-NMR spectrum was obtained using a Bruker Avance 400 MHz spectrometer with a d1 relaxation delay of 30 s to ensure integrals were quantitative. The dissolved API was quantified with respect to the signals from the cation, according to a method described previously.[16]

ATR-FTIR:

The spectra of the supersaturated DMSO/[BuGun][NTf_2]/fenofibrate mixtures were recorded immediately after mixing with DMSO before any crystallization occurred. This was ensured by recording the spectra using a Nicolet 8700 spectrometer with a liquid nitrogen cooled MCT detector on a Golden gate diamond ATR cell, as well as a Smiths Detection IdentifyIR diamond ATR-FTIR equipped with an 100x video microscope of the sample areas. The video microscope on the Smiths Detection diamond ATR-FTIR was used to ensure that no unwanted crystallization or phase separation had occurred at the time of the recording. The spectra obtained on the two instruments was identical, and the high quality spectra of the Nicolet 8700 instrument are the ones presented. All the spectra were ATR corrected using the advanced ATR correction tool in OMNIC 7.

Fenofibrate Crystallization:

In each of the crystallization experiments [BuGun][NTf_2] (2 g), which was freshly dried at 140 °C under vacuum was used. Fenofibrate (0.45 g) and fenofibric acid (0.05 g) were added to the IL at room temperature and the resultant solution stirred until a clear solution was obtained. The antisolvent in the quantity given in Table 3 was then added using a high-precision pipette with stirring, and the solution left stirring overnight to equilibrate. The yields were calculated from the liquid phase after crystallization

using the High Performance Liquid Chromatography (HPLC) procedure below with the purities determined from HPLC analysis of the solid.

HPLC:

The HPLC instrument (Agilent 1100) was equipped with a UV diode array detector. The column used was a YMC-Pack ODS-A 150 × 4.6 mm i.d. column packed with 3 µm particles with 12 nm pore size (YMC America Inc.). The detection wavelength was set at 254 nm. The samples were analyzed using an isocratic method with a 30/70 water/methanol mobile phase containing 0.1% trifluoroacetic acid for 25 mins.

Acknowledgements: The authors thank Novartis for their financial support and Dr. Peter Muller at the MIT single X-ray facility for his services in obtaining the crystal structure of [EtGun][NTf_2]. This research was undertaken, in part, thanks to funding from the Canada Excellence Research Chairs Program.

(1) Welton, T. *Chem. Soc. Rev.* **1999**, *99*, 2071–2083.

(2) Rogers, R. D.; Seddon, K. R. *Science.* **2003**, *302*, 792–793.

(3) Crowhurst, L.; Mawdsley, P. R.; Perez-Arlandis, J. M.; Salter, P. a.; Welton, T. *Phys. Chem. Chem. Phys.* **2003**, *5* (13), 2790.

(4) Schäfer, T.; Rodrigues, C. M.; Afonso, C. a. M.; Crespo, J. G. *Chem. Commun.* **2001**, No. 17, 1622–1623.

(5) Pei, Y.; Wang, J.; Wu, K.; Xuan, X.; Lu, X. *Sep. Purif. Technol.* **2009**, *64* (3), 288–295.

(6) Oppermann, S.; Stein, F.; Kragl, U. *Appl. Microbiol. Biotechnol.* **2011**, *89* (3), 493–499.

(7) Kröckel, J.; Kragl, U. *Chem. Eng. Technol.* **2003**, *26* (11), 1166–1168.

(8) Marques, C. F. C.; Mourão, T.; Neves, C. M. S. S.; Lima, A. S.; Boal-Palheiros, I.; Coutinho, J. a P.; Freire, M. G. *Biotechnol. Prog.* **2013**, *29* (3), 645–654.

(9) Reichert, W. M.; Holbrey, J. D.; Vigour, K. B.; Morgan, T. D.; Broker, G. a.; Rogers, R. D. *Chem. Commun.* **2006**, No. 46, 4767.

(10) Li, X. X.; Xu, X. D.; Dan, Y. Y.; Zhang, M. L. *Crystallogr. Reports* **2009**, *54* (7), 1285–1288.

(11) Li, X.; Xu, X.; Dan, Y.; Feng, J.; Ge, L.; Zhang, M. *Cryst. Res. Technol.* **2008**, *43* (10), 1062–1068.

(12) Liao, J.-H.; Huang, W.-C. *Inorg. Chem. Commun.* **2006**, *9* (12), 1227–1231.

(13) Myerson, A. S. *Handbook of Industrial Crystallization*, 2nd ed.; Butterworth-Heinemann, 2002.

(14) Smith, K. B.; Bridson, R. H.; Leeke, G. a. *J. Chem. Eng. Data* **2011**, *56* (5), 2039–2043.

(15) Resende de Azevedo, J.; Letourneau, J.-J.; Espitalier, F.; Ré, M. I. *J. Chem. Eng. Data* **2014**, *59* (6), 1766–1773.

(16) Weber, C. C.; Kunov-Kruse, A. J.; Rogers, R. D.; Myerson, A. S. *Chem. Commun.* **2015**, *51*, 3649–3657.

(17) Smith, K. B.; Bridson, R. H.; Leeke, G. a. *CrystEngComm* **2014**, *16* (47), 10797–10803.

(18) An, J. H.; Kim, W. S. *Cryst. Growth Des.* **2013**, *13* (1), 31–39.

(19) An, J. H.; Kim, J. M.; Chang, S. M.; Kim, W. S. *Cryst. Growth Des.* **2010**, *1010* (7), 3044–3050.

(20) Swatloski, R. P.; Holbrey, J. D.; Rogers, R. D. *Green Chem.* **2003**, *5* (4), 361.

(21) Swatloski, R. P.; Spear, S. K.; Holbrey, J. D.; Rogers, R. D. *J. Am. Chem. Soc.* **2002**, *134*, 4974–4975.

(22) Paluch, A. S.; Lourenc, T. C.; Han, F.; Costa, L. T. **2016**.

(23) Weber, C. C.; Kulkarni, S. a.; Kunov-Kruse, A. J.; Rogers, R. D.; Myerson, A. S. *Cryst. Growth Des.* **2015**, *15*, 4946−4951.

(24) Klamt, A. *J. Phys. Chem.* **1995**, *99*, 2224–2235.

(25) Cláudio, A. F. M.; Swift, L.; Hallett, J. P.; Welton, T.; Coutinho, J. a P.; Freire, M. G. *Phys. Chem. Chem. Phys.* **2014**, *16* (14), 6593–6601.

(26) Guo, Z.; Lue, B.-M.; Thomasen, K.; Meyer, A. S.; Xu, X. *Green Chem.* **2007**, *9* (12), 1362.

(27) Kahlen, J.; Masuch, K.; Leonhard, K. *Green Chem.* **2010**, *12* (12), 2172.

(28) Klamt, A.; Schüürmann, G. *J. Chem. Soc. Perkin Trans. 2* **1993**, No. 5, 799.

(29) Klamt, a. *Fluid Phase Equilib.* **2000**, *172* (1), 43–72.

(30) Fallanza, M.; González-Miquel, M.; Ruiz, E.; Ortiz, A.; Gorri, D.; Palomar, J.; Ortiz, I. *Chem. Eng. J.* **2013**, *220*, 284–293.

(31) Lee, B.-S.; Lin, S.-T. *Chem. Eng. Sci.* **2015**, *121*, 157–168.

(32) Gonzalez-miquel, M.; Talreja, M.; Ethier, A. L.; Flack, K.; Switzer, J. R.; Biddinger, E. J.; Pollet, P.; Palomar, J.; Rodriguez, F.; Eckert, C. A.; Liotta, C. L. *Ind. Eng. Chem. Res.* **2012**, *51*, 16066−16073.

(33) Pereira, J. F. B.; Flores, L. a.; Wang, H.; Rogers, R. D. *Chem. - A Eur. J.* **2014**, *20*, 15482–15492.

(34) Shimizu, K.; Gomes, M. F. C.; Padua, A. a H.; Rebelo, L. P. N.; Lopes, J. N. C. *J. Phys. Chem. B* **2009**, *113* (29), 9894–9900.

(35) Ab Rani, M. a; Brant, a; Crowhurst, L.; Dolan, a; Lui, M.; Hassan, N. H.; Hallett, J. P.; Hunt, P. a; Niedermeyer, H.; Perez-Arlandis, J. M.; Schrems, M.; Welton, T.; Wilding, R. *Phys. Chem. Chem. Phys.* **2011**, *13* (37), 16831–16840.

(36) Bogdanov, M. G.; Svinyarov, I.; Kunkel, H.; Steinle, C.; Arkhipova, M.; Kantlehner, W.; Maas, G. *Zeitschrift fur Naturforsch. - Sect. B J. Chem. Sci.* **2010**, *65* (7), 791–797.

(37) Jessop, P. G.; Jessop, D. a.; Fu, D.; Phan, L. *Green Chem.* **2012**, *14* (5), 1245.

(38) Zissimos, A. M.; Abraham, M. H.; Klamt, A.; Eckert, F.; Wood, J. *J. Chem. Inf. Comput. Sci.* **2002**, *42* (6), 1320–1331.

(39) Panayiotou, C. *Phys. Chem. Chem. Phys.* **2012**, *14* (11), 3882.

(40) Tsivintzelis, I.; Panayiotou, C. G. In *Handbook of Surface and colloid chemistry*; Birdi, K. ., Ed.; C&C Press, Taylour Francis Group, 2015; pp 145–198.

(41) Thompson, J. E. *A practical Guide to Contemporary Pharmacy Practice*, Thompson,.; Lippincott Williams and Wilkins, 2009.

(42) Knox, C.; Law, V.; Jewison, T.; Liu, P.; Ly, S.; Frolkis, A.; Pon, A.; Banco, K.; Mak, C.; Neveu, V.; Djoumbou, Y.; Eisner, R.; Guo, A. C.; Wishart, D. S. *Nucleic Acids Res.* **2011**, *39*, 1035–1041.

(43) Jondhale, S.; Bhise, S.; Pore, Y. *AAPS PharmSciTech* **2012**, *13* (2), 448–459.

(44) Ag, D.; Ertschenk, B. E. M.; Chulz, B. E. S.; Gmbh, N. C. *Ullmann's encyclopedia of industrial*

chemistry; 2012; pp 175–190.

(45) Carrera, G. V. S. M.; Frade, R. F. M.; Aires-de-Sousa, J.; Afonso, C. a. M.; Branco, L. C. *Tetrahedron* **2010**, *66* (45), 8785–8794.

(46) Bogdanov, M. G.; Petkova, D.; Hristeva, S.; Svinyarov, I. *Zeitschrift für Naturforschung. B, A J. Chem. Sci.* **2010**, *37*, 37–48.

(47) Schlaikjer, C. R. C. Patent application EP001363345A2, 2003.

(48) Olivier-Bourbigou, H.; Magna, L.; Morvan, D. *Appl. Catal. A Gen.* **2010**, *373* (1–2), 1–56.

(49) Gao, Y.; Arritt, S. W.; Twamley, B.; Shreeve, J. M. *Inorg. Chem.* **2005**, *44* (6), 1704–1712.

(50) Phan, L.; Chiu, D.; Heldebrant, D. J.; Huttenhower, H.; John, E.; Li, X.; Pollet, P.; Wang, R.; Eckert, C. A.; Liotta, C. L.; Jessop, P. G. *Ind. Eng. Chem. Res.* **2008**, *47* (3), 539–545.

(51) Gao, H.; Han, B.; Li, J.; Jiang, T.; Liu, Z.; Wu, W.; Chang, Y.; Zhang, J. *Synth. Commun.* **2004**, *34* (17), 3083–3089.

(52) Yu, G.; Chen, X. *J. Phys. Chem. B* **2011**, *115* (13), 3466–3477.

(53) Berg, R. W.; Harris, P.; Riisager, A.; Fehrmann, R. *J. Phys. Chem. A* **2013**, *117* (44), 11364–11373.

(54) Onda, M.; Yoshihara, K.; Koyano, H.; Ariga, K. **1996**, *7863* (12), 8524–8530.

(55) Bannard, R. A. .; Casselman, A. .; Cockburn, W. F.; Brown, G. M. *Can. J. Chem.* **1958**, *36*, 1541.

(56) Ariga, K.; Kamino, A.; Koyano, H.; Kunitake, T. *J. Mater. Chem.* **1997**, *7*, 1155–1161.

(57) David, P.; Mayan, H.; Cohen, H.; Tal, D. M.; Karlish, S. J. *J. Biol. Chem.* **1992**, *267* (2), 1141–1149.

(58) Salunke, D. .; Vijayan, M. *Int. J. petide protein Res.* **1981**, *18*, 348–351.

(59) Davis, T. L.; Elderfield, R. C. *J. Am. Chem. Soc.* **1932**, *54*, 1499–1503.

(60) Kamlet, M. J.; Taft, R. . *J. Am. Chem. Soc.* **1976**, *98*, 377–383.

(61) Abraham, M. H. *Chem. Soc. Rev.* **1993**, *22*, 73–83.

(62) Niedermeyer, H.; Ashworth, C.; Brandt, A.; Welton, T.; Hunt, P. a. *Phys. Chem. Chem. Phys.* **2013**, *15* (27), 11566–11578.

(63) Kurnia, K. a.; Lima, F.; Cláudio, A. F. M.; Coutinho, J. a. P.; Freire, M. G. *Phys. Chem. Chem. Phys.* **2015**, *17*, 18980–18990.

(64) Dickinson, S. R.; Müller, P.; Tanski, J. M. *Acta Crystallogr. Sect. E Crystallogr. Commun.* **2015**, *71* (7), o523–o524.